Available online at www.sciencedirect.com
ScienceDirect
Journal of Loss Prevention in the Process Industries 20 (2007) 337–348
Journal of Loss Prevention in the process industries
www.elsevier.com/locate/jlp

Explosion temperatures and pressures of metals and other elemental dust clouds

Kenneth L. Cashdollar*, Isaac A. Zlochower

Pittsburgh Research Laboratory, National Institute for Occupational Safety and Health, P.O. Box 18070, Cochrans Mill Road, Pittsburgh, PA 15236, USA

Received 1 December 2006; received in revised form 30 April 2007; accepted 30 April 2007

Abstract

The Pittsburgh Research Laboratory of the National Institute for Occupational Safety and Health (NIOSH) conducted a study of the explosibility of various metals and other elemental dusts, with a focus on the experimental explosion temperatures. The data are useful for understanding the basics of dust cloud combustion, as well as for evaluating explosion hazards in the minerals and metals processing industries. The dusts studied included boron, carbon, magnesium, aluminum, silicon, sulfur, titanium, chromium, iron, nickel, copper, zinc, niobium, molybdenum, tin, hafnium, tantalum, tungsten, and lead. The dusts were chosen to cover a wide range of physical properties—from the more volatile materials such as magnesium, aluminum, sulfur, and zinc to the highly "refractory" elements such as carbon, niobium, molybdenum, tantalum, and tungsten. These flammability studies were conducted in a 20-L chamber, using strong pyrotechnic ignitors. A unique multiwavelength infrared pyrometer was used to measure the temperatures. For the elemental dusts studied, all ignited and burned as air-dispersed dust clouds except for nickel, copper, molybdenum, and lead. The measured maximum explosion temperatures ranged from ~1550 K for tin and tungsten powders to ~2800 K for aluminum, magnesium, and titanium powders. The measured temperatures are compared to the calculated, adiabatic flame temperatures.
Published by Elsevier Ltd.

Keywords: Dust; Metal; Explosion; Temperature

1. Introduction

This paper will concentrate on the explosion characteristics of metal and nonmetal elemental dusts. These dusts are important from both the practical and fundamental points of view. These metal and nonmetal elements are often used or occur in industry as powders or dusts, and an evaluation of their possible explosion hazards is important. In addition, the elemental dusts are ideal for studying the fundamental physicochemical processes occurring during combustion because they are pure, uniform substances with well-characterized phase transitions and thermodynamic properties. This is in marked contrast to the complex structures and heterogeneous chemistry associated with the combustion of carbonaceous materials such as coal and grain dusts. The elemental dusts also display a marked variation of reaction exothermicities in air and an enormous range in vapor pressures at their respective flame temperatures.

In the 1960s and earlier, the US Bureau of Mines at Pittsburgh studied the explosibility of metal dusts using a cylindrical 1.2-L Hartmann chamber (Jacobson, Cooper, & Nagy, 1964) with an electric spark ignition source. More recent Pittsburgh Research Laboratory (PRL) studies used a nearly-spherical 20-L chamber and much stronger pyrotechnic ignitors to study the explosibility of metal and other elemental dusts (Cashdollar, 1994; Hertzberg, Zlochower, & Cashdollar, 1991, 1992). The current paper is a continuation of these PRL[1] studies, with an emphasis on experimental explosion temperatures measured with a six-channel infrared (IR) pyrometer. The current paper is also complementary to an earlier experimental study of coal dust explosion temperatures (Cashdollar & Hertzberg,

*Corresponding author. Tel.: +1 412 386 6753; fax: +1 412 386 6595.
E-mail address: KCashdollar@cdc.gov (K.L. Cashdollar).

[1]The majority of this research was conducted in the early 1990s when the PRL was part of the US Bureau of Mines before its transfer to the National Institute for Occupational Safety and Health (NIOSH) in 1996.

0950-4230/$ - see front matter Published by Elsevier Ltd.
doi:10.1016/j.jlp.2007.04.018

1983), using the same IR pyrometer. Other explosion characteristics measured for the metal and other elemental dusts included minimum explosible concentrations (MECs) (lean flammable limits), maximum explosion pressures, and rates of pressure rise. In this paper, the terms "flammability" and "explosibility" are used interchangeably to refer to the ability of an airborne dust cloud to propagate an explosion after it has been initiated by a sufficiently strong ignition source. The explosions observed were rapid deflagrations, not detonations. The IR temperatures and other experimental explosion data provide evidence to evaluate the general mechanisms of homogeneous versus heterogeneous combustion of these elemental dusts. Some preliminary metal explosion temperature data for iron dust are in Cashdollar (1994, 2000).

2. Experimental equipment and test procedures

The dust flammability experiments in this paper were conducted in the PRL 20-L laboratory chamber (Cashdollar, 1994; Cashdollar & Hertzberg, 1982a), which has been used extensively to study the explosibility of various dusts. The chamber (Fig. 1) is near-spherical in shape and made of stainless steel, with a pressure rating of 21 bar. The vertical cross-section is merely a schematic that is meant to show the chamber itself and the vertical positioning of the instrumentation; the positions of the instrumentation around the circumference are shown in the horizontal cross-section. The chamber top is hinged and opens across the full chamber diameter. The hinged top is attached by six $\frac{3}{4}$-in (19-mm) diameter bolts which are not shown in the drawings. Two PRL optical dust probes (Cashdollar, Liebman, & Conti, 1981; Liebman, Conti, & Cashdollar, 1977) were used to measure the uniformity of the dust dispersion at the positions shown in Fig. 1. The optical probes measured the transmission through the dust cloud. Thin jets of air kept the probe windows dust-free. For the majority of the tests, one dust probe with a 38-mm path length and a second dust probe with a 95-mm path length were used. The longer path length is more suitable for dusts with higher densities and larger particle sizes. The strain gauge pressure transducer measured the absolute explosion pressure and rate of pressure rise.

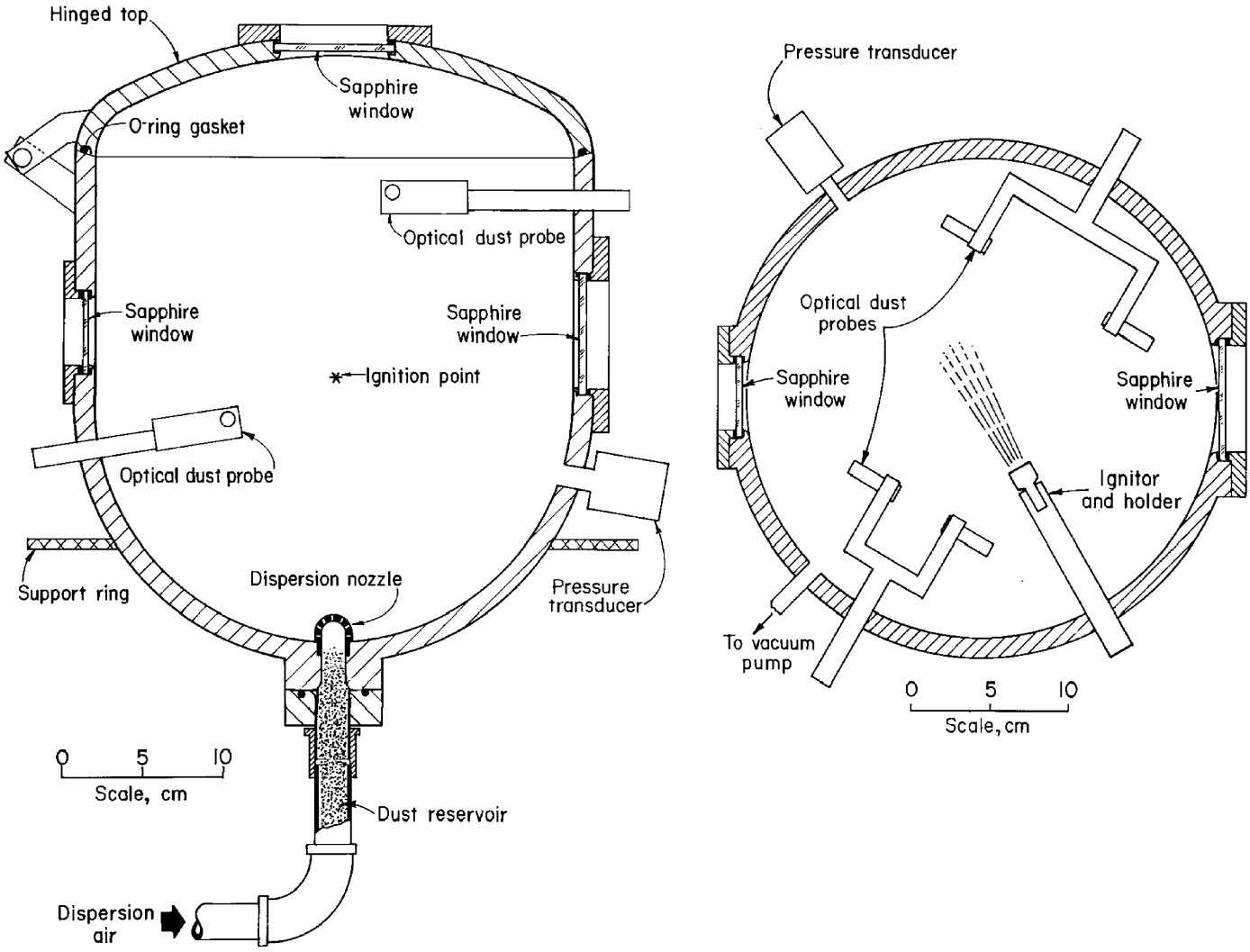

Fig. 1. Vertical and horizontal cross-sections of the 20-L explosibility test chamber.

The patented six-channel IR pyrometer (Cashdollar & Hertzberg, 1982b; Cashdollar, Hertzberg, & Litton, 1979) measured the explosion temperatures by observing the flame radiation through the sapphire window in the top of the 20-L chamber. The pyrometer uses room temperature lead selenide photoconductive detectors and IR interference filters to measure flame radiation simultaneously at six wavelengths: 1.57, 2.30, 3.84, 4.42, 4.57, and 5.00 μm. The pyrometer was calibrated over the temperature range 1200–1450 K using a large blackbody furnace. The linearity of the detectors was confirmed at even higher radiation levels, allowing the extrapolation to higher temperatures. The pyrometer measured the continuum radiation and therefore the temperature of the particles in the flame. The temperature of the gases may have been higher. The experimental particle temperature was calculated by fitting the measured flame radiation data to the Planck equation as modified for nonblackbodies (Cashdollar & Hertzberg 1982b; Menzel, 1955):

$$H = \frac{2a\varepsilon hc^2}{\lambda^5}\left[\exp\left(hc/\lambda kT\right) - 1\right]^{-1}, \quad (1)$$

where H is the observed radiation, a is an adjustable scale factor, ε is the gray emissivity, h is Planck's constant, c is the speed of light, λ is the wavelength, k is Boltzmann constant, and T is the absolute temperature. The combined scale factor $a\varepsilon$ is dependent on the flame emissivity, the fraction of the viewfield filled by the flame, the transmission through any unburned dust on the sapphire window, and the detector sensitivity which varies with ambient temperature. Additional details on the IR pyrometer and the Planck curve fitting procedure are in Cashdollar and Hertzberg (1982b). The advantages of this multiwavelength pyrometer are that temperatures can be calculated without knowing the flame emissivity and that observations can be made through windows that are partially obscured by unburned dust. This pyrometer has been previously used to measure explosion temperatures of coal dust clouds in an 8-L chamber at PRL (Cashdollar & Hertzberg, 1983), and it was also used to measure temperatures of coal dust flames on a flat-flame burner at Brigham Young University (Smoot & Horton, 1978). A similar pyrometer has been used by Mackowski, Altenkirch, Peck, and Tong (1983) to measure temperatures of coal dust flames on a burner.

For each 20-L chamber explosion test, the data from the various instruments were collected by a custom, high-speed personal computer (PC) based data acquisition system (DAS) that has the capability of smoothing the data and searching for peaks. The DAS is programmed to conduct an iterative, nonlinear, least square fit of the pyrometer radiation data to the Planck equation in order to calculate the explosion temperature versus time. The number of pyrometer wavelengths used for the temperature calculation can be varied from three to six. After each explosion test, the pressure, dust probe transmission, and IR temperature data were displayed versus time.

The test procedures for the 20-L chamber are briefly described here. Additional details of the 20-L chamber and test procedures are in Cashdollar (1994) and Cashdollar and Hertzberg (1982a). For most of the tests, the dust was placed on top of the dispersion nozzle rather than in the dust reservoir. After the dust and ignitor were placed in the chamber, the hinged top was closed and bolted, and then the chamber was partially evacuated to an absolute pressure of 0.14 bar, a. Then a 0.3-s blast of dry air (from a 16-L reservoir at 8–9 bar pressure) dispersed the dust and raised the chamber pressure to about 1 bar, a at ignition. The experimental dust concentration reported for the 20-L chamber is the mass of dust divided by the chamber volume. The ignition sources used for the 20-L tests were electrically activated, pyrotechnic ignitors manufactured by Fr. Sobbe[2] of Germany. For the 20-L tests reported in this paper, 2500-J ignitors were used. This is the energy recommended in ASTM E1515 (2006b) for the measurement of minimum explosible dust concentration. The energy is the nominal calorimetric value based on the mass of pyrotechnic powder in the ignitor. The 2500-J ignitor by itself produces a pressure rise of about 0.3 bar in the 20-L chamber.

3. Experimental results and discussion

The metal and nonmetal elemental dusts studied are shown in Fig. 2, highlighted at their positions within the periodic table. Nineteen elements were studied, including boron (B), carbon (C), magnesium (Mg), aluminum (Al), silicon (Si), sulfur (S), titanium (Ti), chromium (Cr), iron (Fe), nickel (Ni), copper (Cu), zinc (Zn), niobium (Nb), molybdenum (Mo), tin (Sn), hafnium (Hf), tantalum (Ta), tungsten (W), and lead (Pb). The dusts highlighted by cross-hatching (Ni, Cu, Mo, and Pb) are the dusts that did not ignite. Table 1 lists the pertinent physical data for the dusts. The first columns list the atomic number, elemental symbol, and name, with a sample number listed for elements that were tested at more than one particle size. The next column lists the density for each element. The size data are listed in three ways. D(SEM) is an estimate of the size range for each dust as observed with a scanning electron microscope. Next is the surface mean diameter as calculated (Cashdollar et al., 1981) from transmission measurements made with the optical dust probes in the 20-L chamber, using the following equation:

$$\tau = \exp\left(\frac{3QC_m}{2\rho D_S}\right), \quad (2)$$

where τ is the transmission, Q is the extinction coefficient, C_m is the mass concentration, ρ is the density of a particle, and D_S is the surface mean diameter of the dust particles. The last column lists the estimated median diameter from a

[2]Mention of any company or product does not imply endorsement by NIOSH.

combination of SEM, dust probe, and other size data (sieving and Coulter Counter analyses).

Scanning electron photomicrographs of six of the elemental dusts are shown in Fig. 3. A 10 μm size marker is shown at bottom center of each photomicrograph. The magnesium (Mg) in Fig. 3(A) is a flake. The aluminum (Al-3) in Fig. 3(B), the iron (Fe-1) in Fig. 3(D), and the tin (Sn) in Fig. 3(F) contain rounded particles, with many approximately spherical. The titanium (Ti) in Fig. 3(C) contains elongated or rod-like particles. The niobium (Nb) in Fig. 3(E) contains particles with sharp edges. The iron is the finest in size of these six dusts, as shown in the SEM photomicrographs and the listings in Table 1.

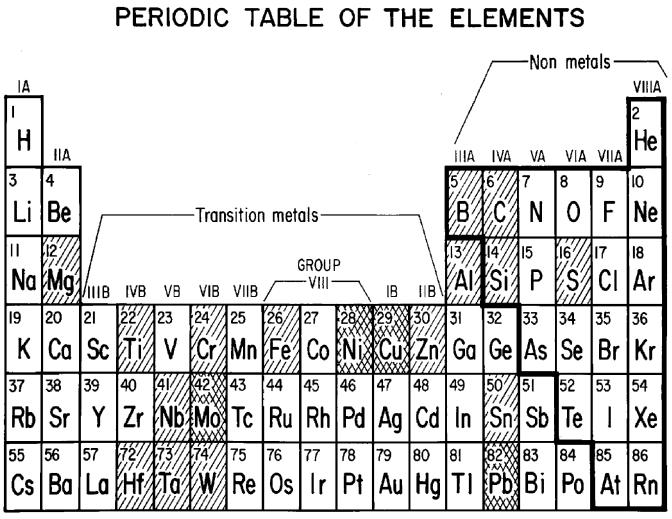

Fig. 2. Periodic table of the elements highlighting the dusts tested.

Examples of the pressure and radiation (at 2.3 μm wavelength) traces versus time are shown in Fig. 4(A) and (B). These are from an iron dust (Fe-1 in Table 1) explosion in the 20-L chamber at a concentration of 600 g/m^3. The radiation reaches its maximum value before peak pressure because the flame front reaches the top window before combustion is completed in the lower parts of the chamber. The calculated temperature and standard deviation in temperature are shown in Fig. 4(C) and (D). The maximum in the temperature trace (1740 K) occurs at the same time as the maximum in radiation, as expected. The standard deviation in the calculated temperature is fairly high at the start of the explosion while the amount of radiation is low. The standard deviation drops to a value of 25 K when the temperature reaches its maximum value.

Fig. 5 shows the curve fits to the Planck equation for four dust explosions at high dust concentrations where the flame would be optically thick. The flame radiation, $H/a\varepsilon$, is plotted versus the wavelength. The respective dust concentrations for the explosions were: 850 g/m^3 for the magnesium (Mg), 800 g/m^3 for the niobium (Nb-1), 900 g/m^3 for the iron (Fe-1), and 1200 g/m^3 for the tin (Sn).

Table 1
Physical data for elemental dusts

Element		Dust	Density, g/cm^3	D(SEM), μm	D_S (%τ), μm	D_{med}, μm
5	B	Boron	2.37	0.5–10	2–6	~3
6	C	Carbon-1	~2.1	0.2–2	⩽2	⩽1
		Carbon-2	~2.1	4–10 f	3–6	~1
		Carbon-3	~2.1	4–30 f	5–7	~4
12	Mg	Magnesium	1.74	10–50 f	30–80	~16
13	Al	Aluminum-1	2.70	3–30 f	~2–4	~1
		Aluminum-2	2.70	5–15	~10–14	~7
		Aluminum-3	2.70	3–60	~40–70	~15
		Aluminum-4	2.70	20–100 r	~60–180	~40
14	Si	Silicon	2.33	1–50	3–8	~4
16	S	Sulfur	2.07	~10–50	~60–100	~35
22	Ti	Titanium	4.54	10–60 r	~30–120	~25
24	Cr	Chromium	7.20	4–40	10–18	~10
26	Fe	Iron-1	7.87	1–8	4–11	~4
		Iron-2	7.87	10–80	~60–160	~45
28	Ni	Nickel-1	8.90	3–8	~30–45	~6
29	Cu	Copper	8.96	10–50	~30–60	~30
30	Zn	Zinc-1	7.13	6–50 f	3–8	~4
		Zinc-2	7.13	10–100 r	~100–200	~45
41	Nb	Niobium-1	8.57	4–50	~30–55	~20
		Niobium-2	8.57	10–60	~50–100	~30
42	Mo	Molybdenum	10.2	3–6	10–23	~5
50	Sn	Tin	5.75	2–20	14–30	~8
72	Hf	Hafnium	13.31	4–30	~7–13	~10
73	Ta	Tantalum	16.6	4–30	~20–60	~15
74	W	Tungsten-1	19.3	⩽1	1–3	⩽1
		Tungsten-2	19.3	5–25	~30–100	~10
82	Pb	Lead	11.3	20–60 r	~100–1000	~40

Note. For the SEM size listing, *f* denotes flake or plate-like particles and *r* denotes rod-like particles.

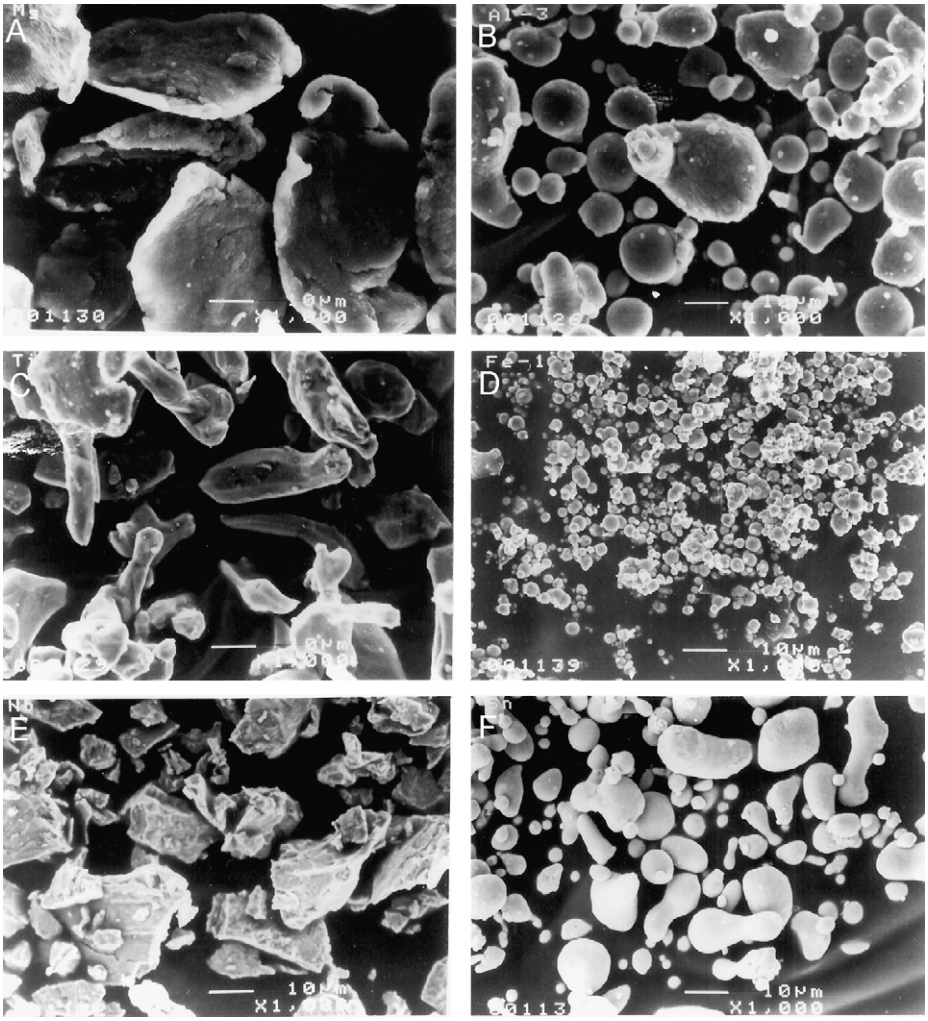

Fig. 3. Scanning electron microscope images of metal dust particles.

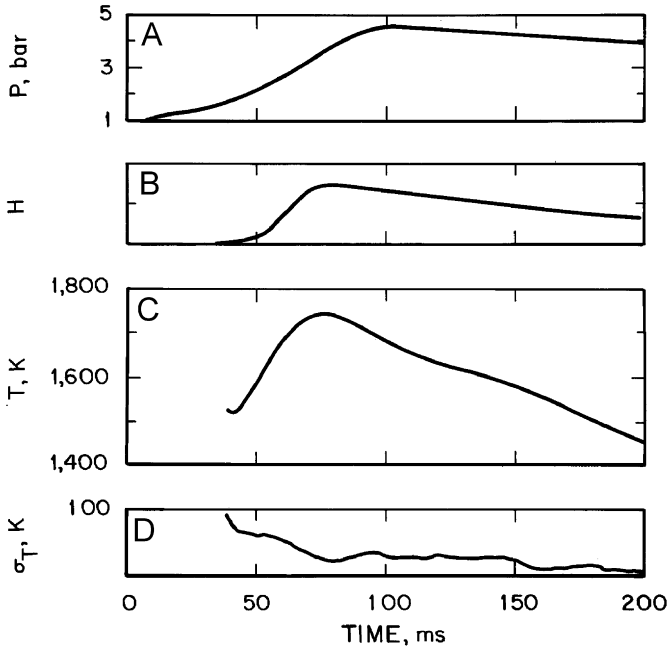

Fig. 4. Pressure, radiation, temperature, and standard deviation in temperature.

The pyrometer radiation data in Fig. 5 were measured at the time of peak flame radiation at the 2.3 μm wavelength for each explosion. All four curves show a good fit of the data points to the Planck curve at a particular temperature. As shown in the figure, the relative radiation values at the two shortest wavelengths have the most effect on the temperature calculation. Of the four dusts, the magnesium explosion had the highest temperature −2740 K, and the niobium had the next highest temperature −2180 K. The iron had a temperature of 1840 K, and the tin had the lowest temperature −1590 K. It should again be noted that these are continuum temperatures of the particles in the explosion flame and that the temperatures of the gases may be higher.

Explosibility data for three aluminum dusts (Al-2, Al-3, and Al-4 from Table 1) as a function of dust concentration are shown in Fig. 6. The data were measured in the 20-L chamber, using 2500-J ignitors. The explosion pressures, rates of pressure rise, and measured explosion temperatures are shown as a function of dust concentration. The absolute explosion pressure data in Fig. 6(C) are the maximum measured explosion pressures (with the pressure rise due to the ignitor subtracted) divided by the starting

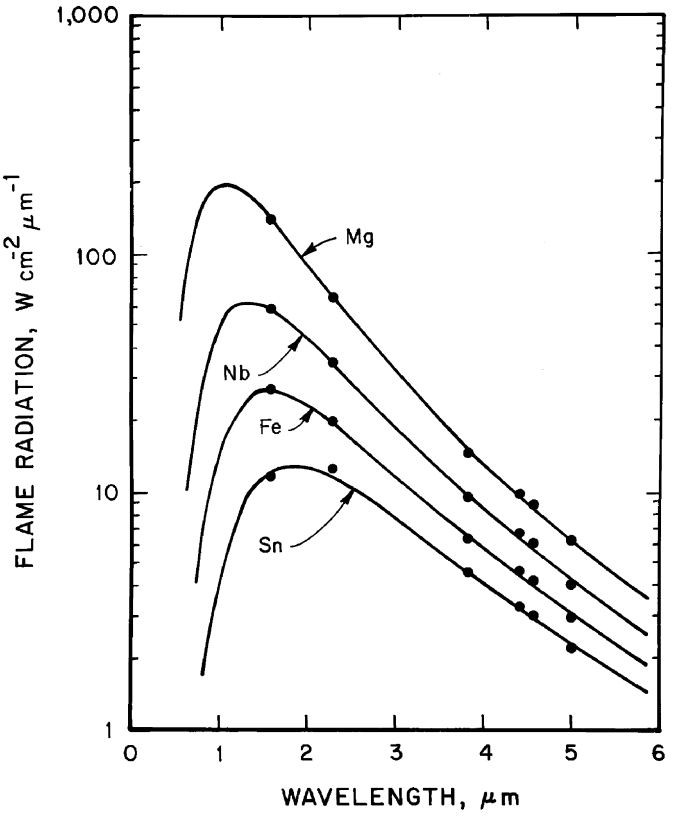

Fig. 5. Radiation versus wavelength for explosions of four metal dusts.

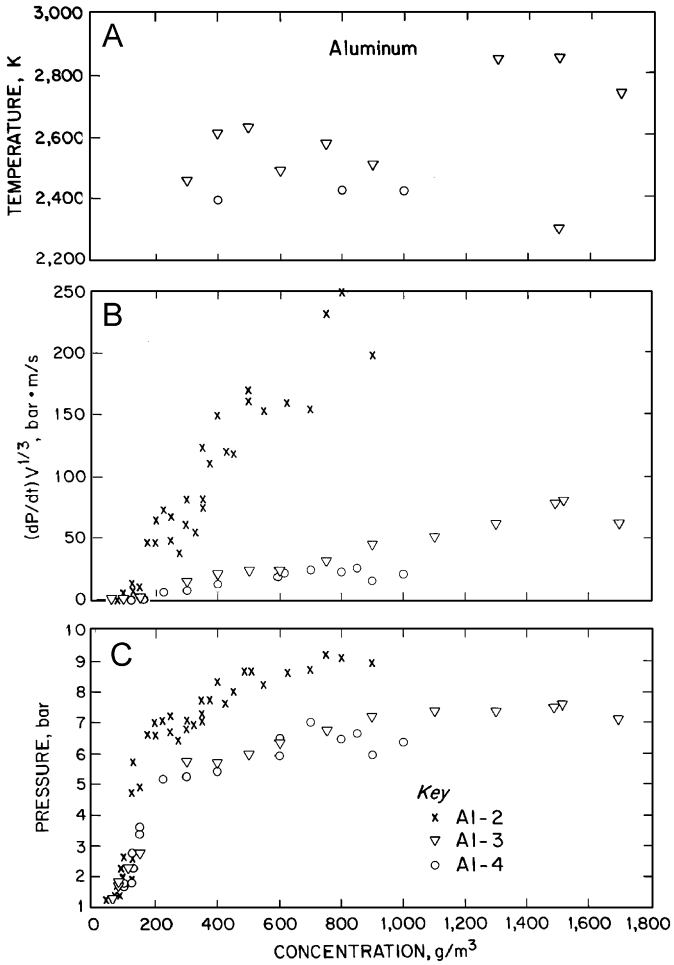

Fig. 6. Explosibility data for three aluminum dusts.

pressure (approximately 1 bar, a). This corrects for small variations in the starting pressure. Fig. 6(B) shows the size normalized maximum rate of pressure rise, $(dP/dt)V^{1/3}$, for each explosion test. Note that the turbulence level is lower in the PRL 20-L chamber than that recommended in ASTM E1226 (2006a) or NFPA 68 (2002), and therefore these $(dP/dt)V^{1/3}$ data are not recommended for vent sizing calculations. The rate of pressure rise data are, however, useful as a relative measure of dust reactivity. For each dust size in Fig. 6, the explosibility data show that explosions are not observed below a certain dust concentration. This is the MEC or lean flammable limit (LFL), which is measured by ASTM E1515 (2006b). The criterion used to determine the MEC value under these test conditions is an absolute explosion pressure of 2 bar, a or, equivalently, a pressure rise of 1 bar. From the data in Fig. 6, the MECs with the 2500-J ignitors for the Al-2, Al-3, and Al-4 dusts are about 90, 90, and 120 g/m^3, respectively. Additional MEC data at 5000-J ignitor energy for these and other dusts are in Cashdollar (1994). For aluminum, the stoichiometric concentration (for formation of Al_2O_3) is $C_{stoich} = 310$ g/m^3. The explosion pressure and $(dP/dt)V^{1/3}$ do not reach their maximum values until concentrations well above C_{stoich} for the aluminum dust. At even higher dust concentrations, both P_{max} and $(dP/dt)_{max}V^{1/3}$ level off as all of the oxygen in the chamber is consumed. However, the dusts show no evidence of a "normal" rich limit as would be observed for flammable gases. It should be noted that the efficiency of the dust dispersion is more uncertain at the higher dust concentrations. The maximum explosion pressure and rate of pressure rise are slightly higher for the Al-3 dust than for the larger Al-4 dust. The even finer sized Al-2 dust has a significantly higher maximum explosion pressure and much higher rate of pressure rise than the other two aluminum dusts. The data (not shown in the figure) for the finest sized Al-1 dust were even higher.

The explosion temperatures shown in Fig. 6(A) were measured with the six-wavelength IR pyrometer. The pyrometer observed the continuum radiation from the particles, and temperatures were calculated from the best Planck curve fit to the IR radiation data. The temperature data shown in Fig. 6(A) were calculated at the time of maximum radiation. This was generally also the time when the standard deviation of the fit to the Planck curve was smallest and the time when the measured temperature was highest. The time of maximum radiation was usually earlier than the time of maximum pressure and probably corresponded to the time when the flame front reached the top sapphire window. The maximum measured particle temperatures for the Al-3 dust were ~2800 K, well below the maximum calculated adiabatic temperature,

$T_{ad,max} = 4060\,K$, for ideal combustion at constant volume. The maximum measured particle temperatures for the Al-4 dust were even lower, although there were only a limited number of measurements for this dust. These experimental temperatures are only those of the particles in the explosion, and the gas temperatures may have been higher. There were no experimental temperatures measured for the two finest sizes of aluminum dust (Al-1 and Al-2) because a sapphire window cracked during early testing of the Al-1 dust, and the windows were replaced with steel blanks for later tests of both of these dusts.

Explosibility data from the 20-L chamber for titanium dust as a function of concentration are shown in Fig. 7. The MEC for this dust is about $70\,g/m^3$, using the 2500-J ignitors. As with the aluminum dusts, the maximum explosion pressures and rates of pressure rise for the titanium dust are at dust concentrations far above the stoichiometric value of $420\,g/m^3$. The maximum measured particle temperatures for the titanium dust were ~2800–3000 K, well below the maximum calculated adiabatic temperature, $T_{ad,max} = 3990\,K$, for ideal combustion. The maximum experimental explosion temperatures for the titanium dust are comparable to those of the Al-3 dust in Fig. 6.

Explosibility data for two iron dusts (Fe-1 and Fe-2 from Table 1) as a function of concentration are shown in Fig. 8. The data were measured in the 20-L chamber, using 2500-J ignitors. The explosion pressures, rates of pressure rise, and measured explosion temperatures are shown as a function of dust concentration as in the previous two figures. From the data in Fig. 8, the MECs for the Fe-1 and Fe-2 dusts are about 220 and $500\,g/m^3$, respectively, using the 2500-J ignitors. However, there is considerable uncertainty in these values, especially for the Fe-2 dust, due to the scatter in the data. For iron, the stoichiometric concentration (for formation of Fe_2O_3) is $C_{stoich} = 650\,g/m^3$. The explosion pressure is close to its maximum value at slightly above C_{stoich} for both iron dusts. However, $(dP/dt)V^{1/3}$ is considerably less than its maximum at C_{stoich} and reaches its maximum value at almost twice C_{stoich} for the Fe-1 dust. At the higher dust concentrations, the maximum explosion pressure, P_{max}, and $(dP/dt)_{max}V^{1/3}$ level off as all of the oxygen in the chamber is consumed and the dusts show no evidence of a "normal" rich limit. It should be noted that the efficiency of the dust dispersion is more uncertain at the higher dust concentrations, particularly for the dusts with higher density. The explosion temperatures shown in Fig. 8(A) were measured with the six-wavelength IR pyrometer at the time of maximum radiation. The maximum measured particle temperatures for the Fe-1

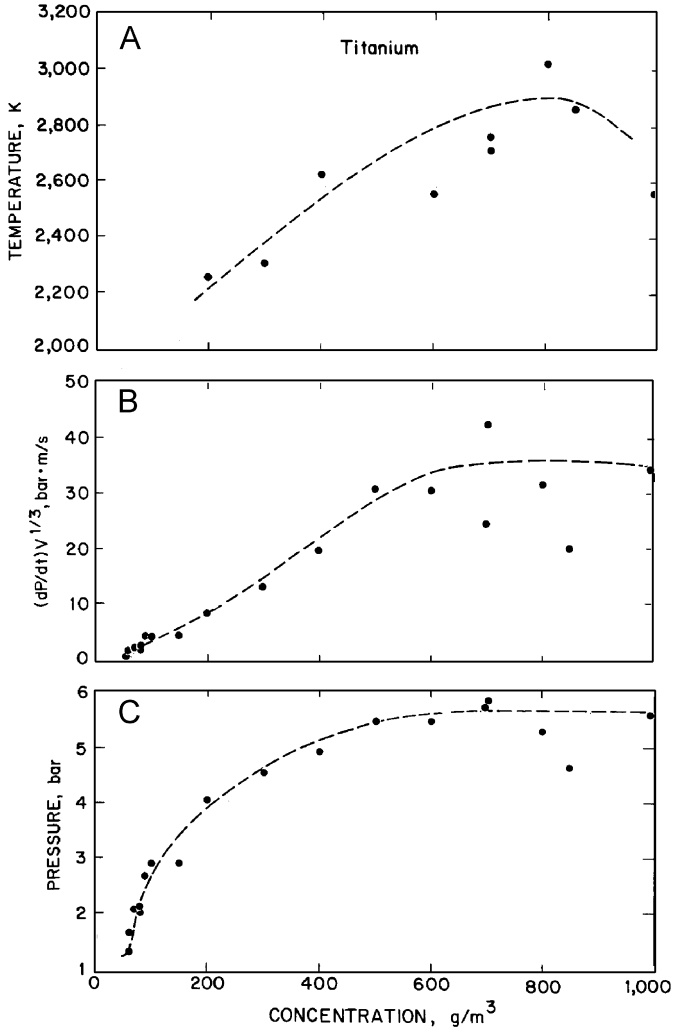

Fig. 7. Explosibility data for titanium dust.

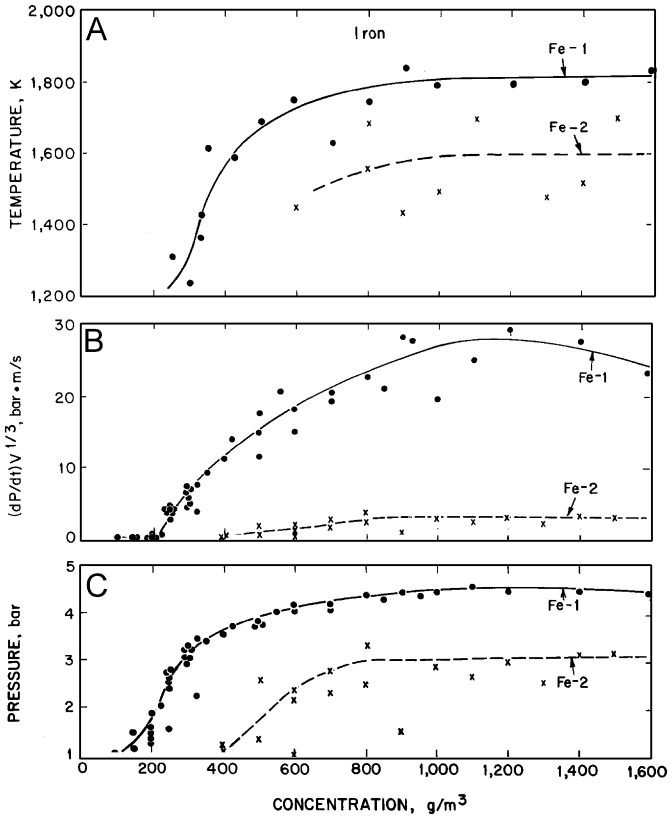

Fig. 8. Explosibility data for two iron dusts.

dust were ~1800 K, well below the maximum calculated adiabatic temperature, $T_{ad,max} = 2490$ K, for ideal combustion at constant volume. The maximum measured particle temperatures for the Fe-2 dust were even lower—about 1500–1700 K. Again, these experimental temperatures are only those of the particles in the explosion, and the gas temperatures may have been different. For all the three explosion characteristics shown in Fig. 8, the Fe-1 dust has higher values than the Fe-2 dust, showing that it is more reactive, due to its finer particle size.

Explosibility data from the 20-L chamber for the two niobium dusts as a function of concentration are shown in Fig. 9. The data were measured in the 20-L chamber, using 2500-J ignitors. The explosion pressures, rates of pressure rise, and measured explosion temperatures are shown as a function of dust concentration as in the previous figures. From the data in Fig. 9, the MECs for the Nb-1 and Nb-2 dusts are about 250 and 420 g/m^3, respectively, using the 2500-J ignitors. However, there is considerable uncertainty in these values, especially for the Nb-2 dust, due to the scatter in the data. For both niobium dusts, the maximum explosion pressure and rates of pressure rise are found at dust concentrations at or above the stoichiometric value of $C_{stoich} = 650$ g/m^3. The explosion temperatures shown in Fig. 9(A) were measured with the six-wavelength IR pyrometer at the time of maximum radiation. The maximum measured particle temperatures for the Nb-1 dust were ~2100 K, well below the maximum calculated adiabatic temperature, $T_{ad,max} = 3540$ K, for ideal combustion. There were no temperature measurements for the Nb-2 dust explosions. As for the other metal dusts, the finer sized niobium dust (Nb-1) appears to be more reactive than the larger Nb-2 dust.

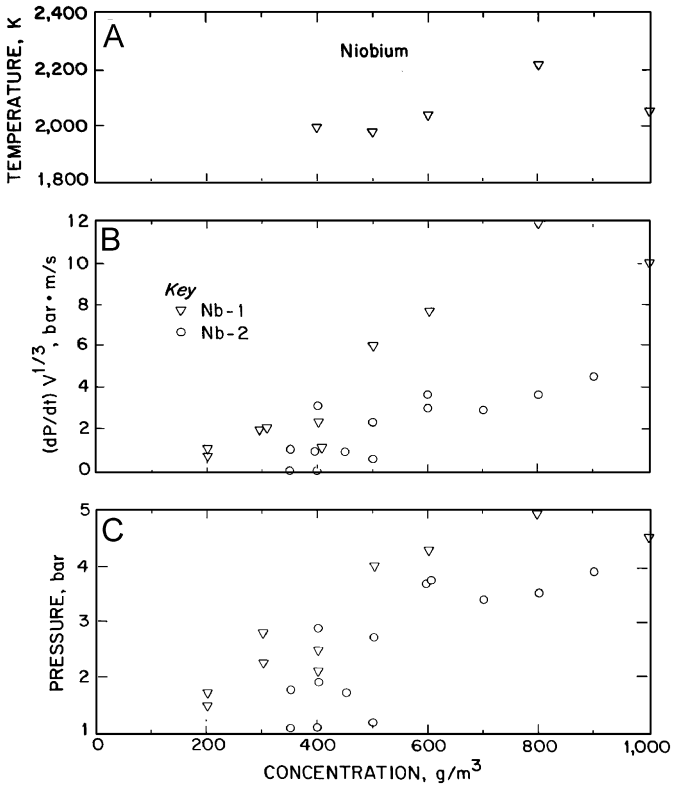

Fig. 9. Explosibility data for two niobium dusts.

Table 2 summarizes the explosibility data for the elemental dusts tested, based on the data curves of Figs. 6–9 and similar data for the other elemental dusts. The first column of the table lists the dust by elemental symbol and sample number. The second column lists the median size from the last column of Table 1. The next column lists the MEC as measured in the 20-L chamber using the 2500-J ignitor. Additional MEC data using a 5000-J ignitor are in Cashdollar (1994) for most of these dusts. The listings of NF (for nonflammable) for the Ni, Cu, Mo, W-2, and Pb dusts were actually determined using the stronger 5000-J ignitor. The next two columns list the calculated ($P_{ad,max}$) and experimental (P_{max}) explosion pressures. The calculated maximum adiabatic explosion pressure is expressed as the ratio of the maximum pressure to the starting pressure. The values were calculated from the NASA-Lewis computer code (McBride & Gordon, 1996) for constant volume combustion, using the thermodynamic properties from the JANAF tables (Chase, Davies, Downey, Frurip, & McDonald, 1985) and the thermodynamic properties of individual substances (TPIS) tables (Gurvich, Veyts, & Alcock, 1991). As discussed in Fig. 6, the listed experimental explosion pressure, P_{max}, is corrected for the pressure rise of the ignitor and normalized to a starting pressure of 1 bar, a. For the experimental explosion pressure, the values listed in Table 2 are the average of the highest three to six data points for each dust. Note that some of the experimental MEC and P_{max} values have been revised from those reported in Cashdollar (1994) and Hertzberg et al. (1992), based on additional data.

The sixth column lists the concentration, $C_{ad,max}$, at which the calculated adiabatic temperature, $T_{ad,max}$, (seventh column) is a maximum. The $C_{ad,max}$ values are generally somewhat higher than the C_{stoich} values. The adiabatic temperature is also calculated from the NASA-Lewis computer code (McBride & Gordon, 1996) for constant volume combustion. The calculated adiabatic temperatures listed in Cashdollar (1994) and Hertzberg et al. (1992) were for constant pressure combustion, which was more appropriate for studying the MECs (lean flammability limits).

The eighth column lists the ideal equilibrium vapor pressures of the elements at the maximum adiabatic flame temperatures that are calculated using standard thermodynamic tables of the Gibbs free energy of the condensed phases and the product vapors. These values are from the JANAF tables (Chase et al., 1985) and the TPIS tables (Gurvich et al., 1991). That vapor pressure is given by

$$P_{equil}(\text{bar}) = 1.01 \exp\left(-\frac{\Delta G_v - \Delta G_c}{RT}\right), \quad (3)$$

where $\Delta G_v - \Delta G_c$ refers to the free energy difference between the vapor and condensed phases, R is the gas

Table 2
Explosibility data for elemental dusts

Dust	D_{med}, μm	MEC, g/m^3	$P_{ad,max}$ ratio	P_{max}, bar, a	$C_{ad,max}$, g/m^3	$T_{ad,max}$, K	P_{equil}, bar at $T_{ad,max}$	β, fraction evaporated at $T_{ad,max}$	$T_{pyrometer}$, K
B	~3	~110	10.5	7.0	130	3300	0.027	>1	1700±100
C-1	⩽1	90	9.4	5.5	120	2670	7×10^{-6}	0.006	1700±100
C-2	~1	F	9.4	~5	120	2670	7×10^{-6}	0.006	1750±100
C-3	~4	NF	9.4	1.1	120	2670	7×10^{-6}	0.001	NF
Mg	~16	55	15.7	8.5	530	3610	~10^3	≫1	2800±100
Al-1	~1	85	12.4	9.4	330	4060	50	≫1	–
Al-2	~7	90	12.4	9.0	330	4060	50	≫1	–
Al-3	~15	90	12.4	7.5	330	4060	50	≫1	2800±100
Al-4	~40	120	12.4	6.6	330	4060	50	≫1	2400±100
Si	~4	200	11.0	7.7	300	3240	0.36	>1	~2300±100
S	~35	100	7.9	5.0	280	2360	57	≫1	–
Ti	~25	70	11.6	5.7	520	3990	3.4	>1	2850±150
Cr	~10	~F	9.0	~3	610	3170	2.6	>1	1850±50
Fe-1	~4	220	6.8	4.5	1000	2490	0.029	>1	1800±50
Fe-2	~45	~500	6.8	3.1	1000	2490	0.029	0.3	~1600±100
Ni	~6	NF	6.7	1.0	900	2400	0.010	0.8	NF
Cu	~30	NF	4.2	1.0	~2200	1520	1.3×10^{-5}	0.0002	NF
Zn-1	~4	300	8.2	4.4	1300	2070	14	≫1	1750±60
Zn-2	~45	~NF	8.2	⩽2		2070	14	≫1	~NF
Nb-1	~20	F	10.0	4.6	800	3540	7×10^{-4}	0.02	2100±100
Nb-2	~30	~420	10.0	~3.7		3540	7×10^{-4}	0.01	–
Mo	~5	NF	7.7	1.0	600	2660	4×10^{-6}	0.0004	NF
Sn	~8	~450	7.1	4.3	1100	2250	0.032	>1	1550±50
Hf	~8	~180	13.5	5.2	1600	4850	0.73	>1	2400±60
Ta	~10	~400	10.6	~4	1300	3760	2.6×10^{-4}	0.006	2350±100
W-1	⩽1	~700	8.7	~3.3	1100	3100	2.3×10^{-7}	8×10^{-5}	1550±50
W-2	~10	NF	8.7	1.0	1100	3100	2.3×10^{-7}	8×10^{-6}	NF
Pb	~40	NF	5.2	1.1	3600	1830	0.33	>1	NF

Notes. NF means the dust was nonflammable or nonignitable. *F* means the dust was flammable but MEC could not be determined.

constant, and T is the calculated adiabatic flame temperature in Kelvin.

The ninth column gives an estimate of β, the maximum fraction of the element that is evaporated in the flame at the calculated maximum temperature. That estimate is based on the ideal evaporation rate into an effective vacuum given by the Hertz–Knudsen equation (Nesmeyanov, 1963). The further assumption of a flame residence time of 0.01 s gives:

$$\beta = 2.6\frac{P_{equil}}{d_p\rho}\left(\frac{M}{T}\right)^{1/2}, \quad (4)$$

where M is the gram-atomic or molecular mass of the vapor species, T is the flame temperature, d_p is the particle diameter and ρ is the particle density (Hertzberg et al., 1992).

The β-values so calculated are idealized estimates where the rate of evaporation in a reactive medium is taken to be equivalent to a vacuum in terms of an assumption of no vapor recondensation. The calculated flame temperature is also an idealized value which assumes perfect mixing, equilibrium conditions, and no heat loss to the walls. Because the assumed flame residence time of 0.01 s is only an estimate, the calculated β-factor should be considered an order of magnitude estimate of the relative volatilities of the elements at the ideal maximum flame temperature. It is clear from the listed values in Table 2 that most of the elements should be totally volatilized at their maximum flame temperatures. The exceptions are carbon, niobium, molybdenum, tantalum, and tungsten—the most refractory elements, which have only a small fraction of material volatilized. Copper also has a very low volatility, but that is due to its low calculated flame temperature. The larger size of the iron (Fe-2) and the nickel are partially volatilized.

The last column in Table 2 lists the experimental IR particle temperature, $T_{pyrometer}$, in Kelvin. As for the experimental explosion pressure, the experimental temperature value listed in Table 2 is the average of the highest three to six data points for each dust. The uncertainty listed for the temperature values is based on the scatter in the data for multiple tests. The standard deviation for the fit to the Planck equation for an individual test was generally about half that value. There may be some additional uncertainty in the experimental temperatures listed in Table 2 due to the extrapolation of the blackbody calibration of the pyrometer for the higher temperatures or to the possible nongray emissivity of the dust explosion.

It should be emphasized that the IR temperatures are for the particles in the flame and that the gas temperatures may be higher, especially for the more easily vaporized dusts.

As mentioned in the discussion of Fig. 6, experimental temperatures were not measured for the two finest sizes of aluminum dust (Al-1 and Al-2) because a sapphire window had cracked during early testing of the Al-1 dust, and the windows were replaced with steel blanks for later tests of these dusts. These two aluminum dusts had much faster rates of pressure rise than any of the other dusts (Cashdollar, 1994). The listed IR temperatures for the Al-3 and Al-4 in Table 2 are based on the temperatures of the aluminum metal particles in the flame because the combustion product, Al_2O_3, is transparent at all of the IR pyrometer wavelengths. The listed temperature of 2800 ± 100 K for the Al-3 is the highest temperature that can be measured for the aluminum particles because the boiling point of aluminum is 2740 K (Weast, 1988) to 2800 K (Chase et al., 1985).

For many of the metals, the observed IR temperatures are those of the incompletely volatilized metal particles since the metals have higher emissivities than the product oxides, which are often transparent in part or all of the IR spectrum. There is no listed IR temperature for the Nb-2 dust because there was insufficient material to measure the explosion temperature at high dust concentrations. Experimental particle temperatures were not measured for the sulfur dust because sulfur vaporizes at a low temperature and the combustion product is a gas.

Four of the elemental dusts (Ni, Cu, Mo, and Pb) listed in Table 2 could not be ignited, even with a 5000-J ignitor. These four dusts showed almost no pressure rise beyond that of the ignitor. It is not surprising that the Cu and Pb did not ignite because their $C_{ad,max}$ values are very high and their $T_{ad,max}$ values are probably too low to sustain flame reaction. The Ni and Mo have reasonably high $T_{ad,max}$ values, similar to that of Fe and higher than those of zinc and tin, but the rate of reaction may be too slow to sustain flame propagation. The larger sizes of several other dusts (C-3, Zn-2, and W-2) could not be ignited, although the Zn-2 showed some slight activity in some of the tests.

The dust with the lowest $T_{ad,max}$ value that produced explosions was zinc with $T_{ad,max} = 2070$ K. However, the Zn is easily vaporized at flame temperatures. Considering its low $T_{ad,max}$ value, it is not surprising that the larger size of Zn could not be reproducibly ignited with the 2500-J ignitor.

For most of the experimental temperature calculations in Table 2, all six pyrometer channels were used (see Fig. 5), but in some cases only channels 1, 2, 3, and 6 or channels 1, 2, and 3 were used. For most of the elemental dusts, the emissivity was high. However, for the Si and Ta, the calculated emissivity was low (~0.1). For three dusts (B, Si, and Hf), only the first three pyrometer wavelengths were used to calculate the temperatures, because of higher emissivity at the three longer wavelengths. Because of this, the temperatures for the boron, silicon, and hafnium are more uncertain than those of the other dusts. For the silicon, the combustion product SiO_2 would be transparent at the shorter IR wavelengths and opaque at the longer IR wavelengths. Therefore, the temperature measurement from the three shorter wavelengths would be the temperature of the silicon metal. The radiation at the longer three wavelengths would be a combination of radiation from the Si metal and SiO_2 metal oxide.

4. Conclusions

A summary comparison of the experimentally measured explosion pressures (P_{max}) and the calculated adiabatic pressures ($P_{ad,max}$) from Table 2 is shown in Fig. 10. The data points for the dusts are identified by the elemental symbols. The lines identify values at 40%, 60%, 80%, and 100% of the calculated adiabatic pressures. The dusts whose experimental pressures are closest to the calculated adiabatic values are B, Al-1, Al-2, Si, and Fe-1. These are also among the finest sized dusts, with median diameters below 10 μm.

A summary comparison of the experimentally measured explosion temperatures ($T_{pyrometer}$) and the calculated

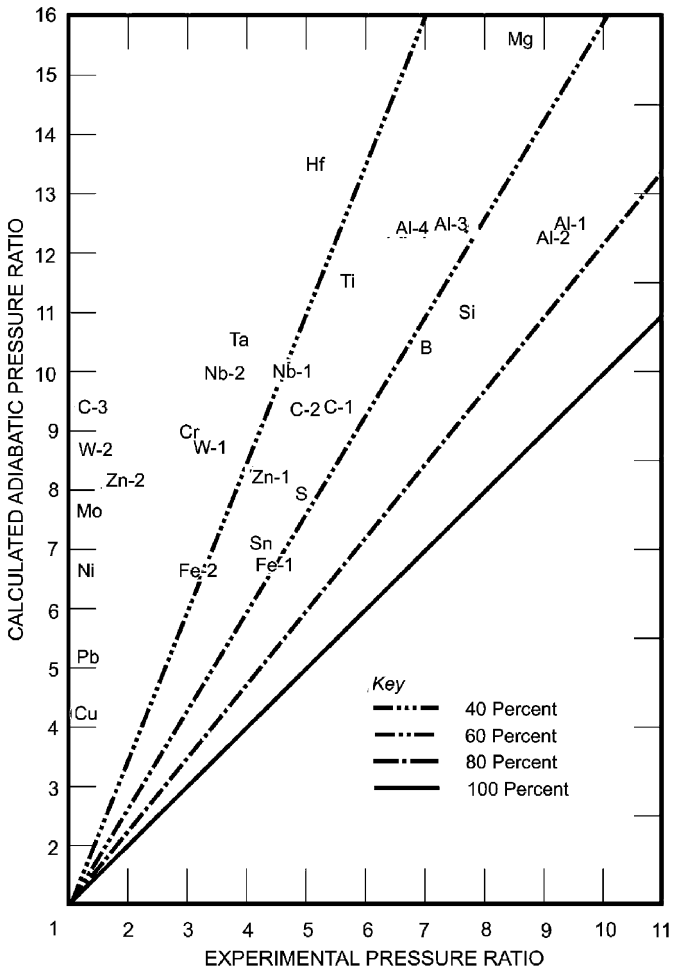

Fig. 10. Comparison of calculated and experimental explosion pressures, with data points shown as element symbols.

adiabatic temperatures ($T_{ad,max}$) from Table 2 is shown in Fig. 11. The data points for the dusts are identified by the elemental symbols. The lines identify values at 40%, 60%, 80%, and 100% of the calculated adiabatic temperatures. The two dusts whose experimental temperatures are closest to the $T_{ad,max}$ values are Zn-1 and Mg. These are also two of the dusts that are the most easily vaporized (see Table 2).

The aluminum (Al-3), silicon, titanium, iron (Fe-1), and tin also have high volatilities at their flame temperatures. These dusts have measured explosion temperatures that are at an intermediate position in the figure, at about 70% $T_{ad,max}$. Two of the dusts with high volatilities, boron and hafnium, have experimental temperatures that are only about half of the $T_{ad,max}$-values. These were also dusts that had a larger than normal uncertainty in their temperature measurements, as discussed in the previous section. The flammable dusts (C, Nb, Ta, and W) that have very low volatilities are also those whose measured explosion temperatures are among the farthest from their $T_{ad,max}$ values.

For dusts that were tested at more than one particle size, the experimental temperatures of the finer sizes were closer to the calculated temperatures, as expected. The larger sizes of aluminum (Al-4) and iron (Fe-2) had measured temperatures that were farther from the adiabatic values than the temperatures for the finer sizes. The two sizes of carbon (C-1 and C-2) that produced explosions had about the same measured temperatures, but both were very fine sizes.

In general, the dusts whose experimental temperatures are closer to the adiabatic values are those with the finer particle sizes, those that are more easily vaporized, and/or those that are intrinsically more reactive. However, the boron and hafnium appear to be exceptions since they are both fine size and easily volatilized.

The experimental pressure and temperature data presented here will be useful in evaluating various models of metal dust combustion. Additional information on the mechanisms of metal combustion is in Hertzberg et al. (1992) which discusses the volatility of the metals and in Kanury (1975) which has information on combustion properties of carbon and metals. The results reported in this paper provide information on the combustion characteristics of 19 metal and nonmetal elemental dusts. The experimentally measured temperatures can help in the understanding of the combustion process. However, because of the effects of particle size, these data should not be considered to be representative of all dust samples of these elements. Ideally, explosion temperatures would be measured for identical, small particle sizes of the various elemental dusts in order to study their intrinsic combustion properties, but it would be difficult to obtain these. For the practical use of explosibility data for safety planning, it is important to test the particular size of dust that occurs at a particular industrial plant, rather than trying to extrapolate from other test data for a different size of the same material.

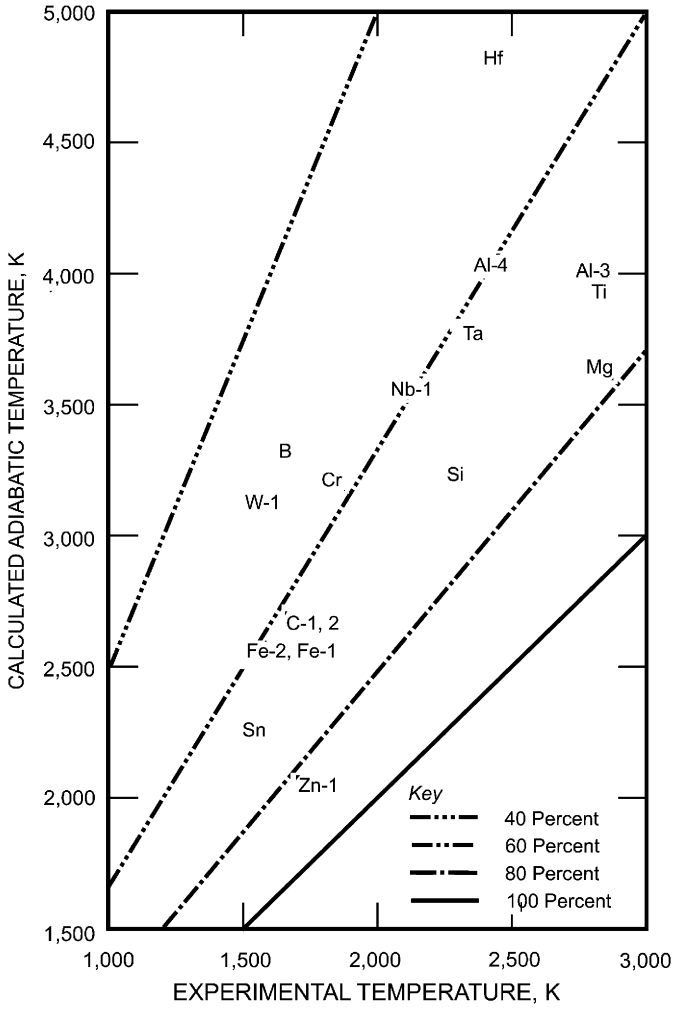

Fig. 11. Comparison of calculated and experimental explosion temperatures, with data points shown as element symbols.

Acknowledgment

The authors acknowledge the assistance of G.M. Green of the PRL in the collection of the experimental data and C.E. Lucci for writing the software code to calculate the explosion temperatures from the pyrometer data.

Disclaimer. The findings and conclusions in this report are those of the authors and do not necessarily represent the views of the National Institute for Occupational Safety and Health.

References

ASTM International. (2006a). Standard test method for pressure and rate of pressure rise for combustible dusts, E1226-00. In Annual book of ASTM standards, Vol. 14.02 (pp. 328–338). West Conshohocken, PA: ASTM International.

ASTM International. (2006b). Standard test method for minimum explosible concentration of combustible dusts, E1515-03. In Annual book of ASTM standards, Vol. 14.02 (pp. 480–488). West Conshohocken, PA: ASTM International.

Cashdollar, K. L. (1994). Flammability of metals and other elemental dusts. *Process Safety Progress*, *13*, 139–145.

Cashdollar, K. L. (2000). Overview of dust explosibility characteristics. *Journal of Loss Prevention in the Process Industries*, *13*, 183–199.

Cashdollar, K. L., & Hertzberg, M. (1982a). 20-L explosibility test chamber for dusts and gases. *Review of Scientific Instruments*, *56*, 596–602.

Cashdollar, K. L., & Hertzberg, M. (1982b). Infrared pyrometers for measuring dust explosion temperatures. *Optical Engineering*, *21*, 82–86.

Cashdollar, K. L., & Hertzberg, M. (1983). Infrared temperatures of coal dust explosions. *Combustion and Flame*, *51*, 23–35.

Cashdollar, K. L., Hertzberg, M., & Litton, C. D. (1979). Multichannel infrared pyrometer. *US Patent 4,142,417*.

Cashdollar, K. L., Liebman, I., & Conti, R. S. (1981). *Three Bureau of Mines optical dust probes* (26pp.). US Bureau of Mines RI 8542.

Chase Jr., M. W., Davies, C. A., Downey Jr., J. R., Frurip, D. J., McDonald, R. A., & Syverud, A. N. (1985). JANAF thermochemical tables (3rd ed.) (Midland, MI: Thermal Group, Dow Chemical USA). *Journal of Physical and Chemical Reference Data*, *14*(Suppl. 1).

Gurvich, L. V., Veyts, I. V., & Alcock, C. B. (1991). *Thermodynamic properties of individual substances* (4th ed., Vol. 2, Parts 1 & 2). New York: Hemisphere Publishing Co.

Hertzberg, M., Zlochower, I. A., & Cashdollar, K. L. (1991). Explosibility of metal dusts. *Combustion Science and Technology*, *75*, 161–165.

Hertzberg, M., Zlochower, I. A., & Cashdollar, K. L. (1992). Metal dust combustion: explosion limits, pressures, and temperatures. In *24th symposium (international) on combustion* (pp. 1827–1835). Pittsburgh: The Combustion Institute.

Jacobson, M., Cooper, A. R., & Nagy, J. (1964). *Explosibility of metal powders* (25pp.). US Bureau of Mines RI 6516.

Kanury, A. M. (1975). *Introduction to combustion phenomena*. New York: Gordon and Breach.

Liebman, I., Conti, R. S., & Cashdollar, K. L. (1977). Dust cloud concentration probe. *Review of Scientific Instruments*, *48*, 1314–1316.

Mackowski, D. W., Altenkirch, R. A., Peck, R. E., & Tong, T. W. (1983). A method for particle and gas temperature measurement in laboratory-scale, pulverized-coal flames. *Combustion Science and Technology*, *31*, 139–153.

McBride, B. J. & Gordon, S. (1996). *Computer program for calculation of complex chemical equilibrium compositions and applications*. NASA Reference Publication 1311.

Menzel, D. H. (1955). *Fundamental formulas of physics*. New York: Prentice-Hall p. 670.

Nesmeyanov, A. N. (1963). In J. I. Carasso (Ed.), *Vapor pressure of the chemical elements*. New York: Academic Press (translated from Russian).

NFPA. (2002). *Guide for venting of deflagrations, NFPA 68*. Quincy, MA: National Fire Protection Association.

Smoot, L. D., & Horton, M. D. (1978). Final report (Vol. 1, 315pp.), US Bureau of Mines Contract G0177034, March 1, 1978, available as OFR 104-82 from Pittsburgh Research Laboratory, Pittsburgh, PA.

Weast, R. C. (Ed.), (1988). CRC handbook of chemistry and physics (69th ed.). Boca Raton, FL: CRC Press.